Pat1 increases the range of decay factors and RNA bound by the Lsm1-7 complex

Joseph H. Lobel[1,2] and John D. Gross[2,*]

[1]Chemistry and Chemical Biology Graduate Program, University of California, San Francisco, San Francisco, California

[2]Department of Pharmaceutical Chemistry, University of California, San Francisco, San Francisco, California

Running title: Pat1 promotes oligomerization of RNA decay factors

Keywords: mRNA decay, Pat1, Lsm1, P-Bodies, Dcp2

*** Correspondence to:**

John D. Gross

University of California

600 16th St Box 2280

San Francisco, CA 94158

jdgross@cgl.ucsf.edu

Voice: (415) 514-4402

Abstract

Pat1 promotes the activation and assembly of multiple proteins during mRNA decay. After deadenylation, the Pat1/Lsm1-7 complex binds to transcripts containing oligo(A) tails, which can be modified by the addition of several terminal uridine residues. Pat1 enhances Lsm1-7 binding to the 3' end, but it is unknown how this interaction is influenced by nucleotide composition. Here we examine Pat1/Lsm1-7 binding to a series of oligoribonucleotides containing different A/U contents using recombinant purified proteins from fission yeast. We observe a positive correlation between fractional uridine content and Lsm1-7 binding affinity. Addition of Pat1 broadens RNA specificity of Lsm1-7 by enhancing binding to A-rich RNAs and increases cooperativity on all oligonucleotides tested. Consistent with increased cooperativity, Pat1 promotes multimerization of the Lsm1-7 complex, which is potentiated by RNA binding. Furthermore, the inherent ability of Pat1 to multimerize drives liquid-liquid phase separation with multivalent decapping enzyme complexes of Dcp1/Dcp2. Our results uncover how Pat1 regulates RNA binding and higher order assembly by mRNA decay factors.

INTRODUCTION

A dense network of protein-protein interactions regulates 5'-3' mRNA decay, which is important for gene expression and many physiological processes including development, microRNA-mediated decay, and quality control mechanisms (Moore 2005; Kurosaki et al. 2019; Mugridge et al. 2018; Jonas and Izaurralde 2015). Bulk 5'-3' mRNA degradation begins with the trimming of the 3' poly(A) tail by cytoplasmic deadenylases, which can be

45 followed by addition of several uridines by terminal uridine transferases in fission yeast
46 and metazoans (Mugridge et al. 2018; Rissland and Norbury 2009; Lim et al. 2014; Yi et
47 al. 2018; Webster et al. 2018). After deadenylation and subsequent uridylation, the
48 heterooctameric Pat1/Lsm1-7 complex assembles on or near the 3' A/U-rich
49 deadenylated tail of the mRNA (Mitchell et al. 2012; Tharun and Parker 2001; Bonnerot
50 et al. 2000; Bouveret et al. 2000; Tharun et al. 2000; Wang et al. 2017). Pat1 subsequently
51 activates decapping by Dcp1/Dcp2, leading to rapid 5'-3' degradation of the mRNA body
52 by the conserved exonuclease Xrn1 (Lobel et al. 2019; Nissan et al. 2010; Stevens 1980;
53 Mugridge et al. 2018; Charenton et al. 2017; Tharun and Parker 2001). Pat1 activates
54 proteins at both the 5' and 3' end of the mRNA by enhancing RNA binding of the Lsm1-7
55 complex to the deadenylated 3' end and decapping by the Dcp1/Dcp2 complex (Lobel et
56 al. 2019; Nissan et al. 2010; Chowdhury et al. 2013; Charenton et al. 2017). Deletion of
57 Pat1 results in accumulation of poorly translated, deadenylated, capped transcripts,
58 suggesting a block in decapping (Wang et al. 2017; He et al. 2018; Tharun and Parker
59 2001).
60
61 Many mRNA decay factors, including Pat1, are enriched in Processing-bodies (P-bodies)
62 which are a class of membraneless organelles that may function in mRNA storage or
63 decay (Teixeira and Parker 2007; Xing et al. 2018; Hubstenberger et al. 2017; Sheth and
64 Parker 2003). At the molecular level, these structures are promoted by multivalent
65 protein-protein and protein-nucleic acid interactions that are required for phase separation
66 (Banani et al. 2017). Overexpression of Pat1 enhances P-body formation in fungi,

67 suggesting its importance in assembling these structures (Wang et al. 2017; Sachdev et
68 al. 2019). Therefore, Pat1 functions at multiple steps during 5'-3' mRNA decay to
69 coordinate degradation of the transcript.
70
71 Pat1 uses a combination of disordered and globular domains to interact with and activate
72 multiple mRNA decay factors. The disordered N-terminus contains a conserved FDF motif
73 that interacts with Dhh1 (DDX6 in humans) and potentiates P-body formation, but is
74 largely dispensable for function (Sachdev et al. 2019; Sharif et al. 2013; Pilkington and
75 Parker 2008). The unstructured middle domain contains multiple short linear interaction
76 motifs (SLiMs) and cooperates with the structured C-terminal domain to activate RNA
77 binding by Lsm1-7 and decapping by the Dcp1/Dcp2 complex through multiple
78 mechanisms (Lobel et al. 2019; Pilkington and Parker 2008; Chowdhury et al. 2013).
79
80 While it is known how Pat1 activates different mRNA decay factors, much less is
81 understood about how it affects specific RNA recognition by Lsm1-7. *In vitro*, budding
82 yeast Pat1/Lsm1-7 shows a preference for oligoadenyated RNAs compared to those
83 containing poly(A) tails; however, genome-wide CLIP studies indicate Pat1/Lsm1 co-
84 occupy the 3' untranslated region (UTR) of budding yeast transcripts without enriching a
85 specific sequence motif (Chowdhury et al. 2007; Mitchell et al. 2012). In fission yeast and
86 metazoan cells, deletion of Lsm1 or Pat1 stabilizes mRNA decay intermediates with
87 oligo(A) tails containing several uridines (Lim et al. 2014; Rissland and Norbury 2009).
88 Furthermore, in mammalian cells, knockdown of Pat1 stabilizes transcripts with AU-rich

sequences in the 3' UTR (Vindry et al. 2017). Lsm1-7 can also bind oligo(U) RNA sequences *in vitro* and promotes decay of histone mRNAs that containing U-rich tails in cells (Mullen and Marzluff 2008; Chowdhury et al. 2007; Wu et al. 2014). How Pat1 affects location and sequence specificity of the Lsm1-7 complex on mRNA is poorly understood.

In this work, we evaluate recombinant purified *S.pombe* Pat1/Lsm1-7 complex binding to a series of oligonucleotides of different A/U content. Lsm1-7 alone has a binding preference for U-rich RNAs. Addition of Pat1, however, broadens the specificity of the Lsm1-7 complex by enhancing binding to A-rich targets. Furthermore, Pat1 increases cooperative binding of Lsm1-7 to oligonucleotides, which drives multimerization of the heterooctamer on RNA in a sequence independent manner. Oligomerization is an inherent property of Pat1 that permits higher order assembly with multivalent Dcp1/Dcp2 complexes, which can recruit additional mRNA decay machinery. Taken together, this work reveals how Pat1 broadens the specificity of Lsm1-7 and promotes the assembly of higher order decapping complexes.

RESULTS

The PatMC/Lsm1-7 complex cooperatively binds to A-rich RNA

Previous studies indicate that the middle and C-terminal domains of Pat1 (termed PatMC) are sufficient to support cell growth in yeast (Pilkington and Parker 2008; Lobel et al. 2019). To understand how different 3' end sequences influence PatMC/Lsm1-7 binding, we tested recombinant purified *S.pombe* Lsm1-7 complexes alone or coexpressed with

PatMC for their ability to bind different oligo-RNAs by fluorescence polarization (**Fig. 1A-B)**. Because global profiling of RNA tails indicate that uridine residues are found on short tails (<25 nt), we investigated a series of 15mers containing different adenine and uracil contents (Chang et al. 2014; Rissland and Norbury 2009). As seen previously, PatMC enhanced the RNA binding of Lsm1-7 to A15 RNA by an order of magnitude (Lobel et al. 2019). The fold-enhancement of Lsm1-7 RNA binding by PatMC strongly correlated with the fractional adenine content of the 15mer, where a greater difference in free energy of binding was observed for more adenine-rich substrates **(Fig. 1C & S1A-F)**. Furthermore, the Lsm1-7 complex alone strongly favored binding to U-rich 15mers, which was not affected by PatMC. Because PatMC does not bind RNA with appreciable affinity on its own, PatMC may serve to selectively enhance RNA binding of Lsm1-7 to adenine rich tails and may be dispensable for engaging U-rich tails (Lobel et al. 2019) (**Fig. S1G**).

In addition to the differences in affinities for the oligonucleotides, we also observed a difference in Hill coefficients, a measure of cooperativity that places a lower bound on the number of Pat1/Lsm1-7 complexes binding RNA. The binding isotherms of the PatMC/Lsm1-7 complex were consistently ~2 fold more cooperative than Lsm1-7 alone for all tested RNAs, suggesting that PatMC/Lsm1-7 may be engaging A15 and U15 RNA in a different manner **(Fig. 1D)**. Specifically, PatMC/Lsm1-7 had a Hill coefficient of ~1 for U15 RNA and ~2 for A15 RNA, suggesting that binding to A15 is cooperative while U15 binding is not. This indicates that at least one or two copies of the PatMC/Lsm1-7 complex cooperatively bind to U15 or A15 RNA, respectively.

Short RNAs are sufficient to promote dimerization of the PatMC/Lsm1-7 complex

To directly test the number of PatMC/Lsm1-7 complexes bound to short oligonucleotides, we used size exclusion chromatography coupled to multiangle light scattering (SEC-MALS). The SEC step fractionates protein complexes by hydrodynamic radius and molar mass is concurrently detected by light-scattering and differential refractometry (Wyatt 1993). The PatMC/Lsm1-7 complex was incubated with stoichiometric amounts of A15 RNA and subjected to SEC-MALS. The A15 RNA promoted the formation of two peaks that had identical protein composition and molar masses corresponding to that of a dimeric (two copies of PatMC/Lsm1-7) and tetrameric assembly **(Fig. 2A, Table 1)**. Shorter RNAs, such as A10, also promoted oligomeric PatMC/Lsm1-7 assemblies, with molar masses corresponding to dimeric and tetrameric complexes **(Fig. 2B)**. However, we observed that the A10 RNA reduced tetramerization and instead produced predominantly dimeric PatMC/Lsm1-7 complexes, based on the relative ratio of the peaks in the chromatogram. This suggests that RNA length many influence tetramerization, but short RNAs still promote higher order assembly of the PatMC/Lsm1-7 complex.

To evaluate the stability of the oligomeric assemblies, we performed sedimentation velocity analytical ultracentrifugation (SV-AUC) on PatMC/Lsm1-7 with stoichiometric amounts of A15 RNA over the course of 12 hours. While we could detect a strong dimeric peak in the sedimentation distribution, there was minimal amounts of tetrameric assemblies **(Fig. 2C)**. Furthermore, the tetrameric fraction of the PatMC/Lsm1-7/A15

155 complex disassembled into dimers and tetramers upon reinjection over a size exclusion
156 column, while the dimeric peak did not further dissociate (**Fig. S2A-C)**. This suggests that
157 the tetrameric PatMC/Lsm1-7/RNA is less stable the dimeric species.
158
159 We next asked how PatMC/Lsm1-7 assembled on U15 RNA. As seen with A15 RNA,
160 addition of stoichiometric amounts of U15 to the PatMC/Lsm1-7 complex resulted in two
161 peaks by SEC-MALS with molar masses corresponding to dimeric and tetrameric
162 assemblies **(Fig. 3A/B)**. This effect depends on PatMC, because Lsm1-7 alone bound to
163 U15 RNA remained monomeric (**Fig. 3C**). Taken together, this indicates that PatMC
164 promotes the higher order assembly of the PatMC/Lsm1-7 complex on both A15 and U15
165 RNA. This suggests that while both A15 and U15 promote dimerization of the
166 PatMC/Lsm1-7 complex, some of the contacts of the dimer may differ, as evidenced by
167 the difference in RNA binding cooperativity (**Fig. 1D**).
168
169 It is possible that that each PatMC/Lsm1-7 complex binds an individual RNA or that
170 multiple PatMC/Lsm1-7 complexes co-occupy a single RNA to promote oligomerization.
171 To test these possibilities, we determined the stoichiometry of PatMC/Lsm1-7 binding to
172 RNA. Experiments were performed under saturating conditions, where concentration of
173 the oligo-RNA was far above the K_d. Binding of labelled U15 was followed by fluorescence
174 anisotropy. Titration of Lsm1-7 alone or the PatMC/Lsm1-7 complex results in saturation
175 of the anisotropy signal at one equivalent of RNA, indicating 1:1 binding between
176 PatMC/Lsm1-7 and the U15 oligonucleotide (**Fig. 3D**). Similar results were obtained for

PatMC/Lsm1-7 binding to A15 (**Fig. S3**). This indicates that each PatMC/Lsm1-7 heterooctamer binds a single oligo-RNA, though we cannot exclude the possibility that PatMC/Lsm1-7 can co-occupy RNA sequences longer than 15nt tested here. Therefore, we conclude that RNA ligands of different sequences and lengths induce stable dimerization of the PatMC/Lsm1-7 complex.

Dimerization is an intrinsic property of the PatMC/Lsm1-7 complex

As PatMC/Lsm1-7 binds to RNA as a higher order assembly, we asked if the complex had the intrinsic ability to multimerize in the absence of RNA. While PatMC/Lsm1-7 initially purified as a monomer, concentration and subsequent SEC-MALS of the complex in the absence of RNA revealed two peaks with molar masses corresponding to monomeric and dimeric PatMC/Lsm1-7 complexes **(Fig. 4A-C)**. This indicates that the PatMC/Lsm1-7 complex has the inherent ability to form multimers independent of nucleic acid, and suggests that RNA may drive higher order assembly.

To test the stability of the assemblies in the absence of RNA, we performed SV-AUC on the PatMC/Lsm1-7 complex alone. Over the course of 12 hours, we observed both a monomeric and dimeric species, indicating that both these complexes were stable **(Fig. 4D)**. Furthermore, increasing salt concentrations favored monomerization of the complex, indicating PatMC/Lsm1-7 oligomerization is reversible **(Fig. S4)**. Because Lsm1-7 was monomeric in the absence of PatMC, the above results indicate PatMC drives multimerization of Lsm1-7, which may be enhanced by RNA binding (**Fig. 2A & 3A)**.

199

200 **PatMC promotes liquid-droplet formation with Dcp2 and recruits additional mRNA**
201 **decay factors**

202 Previous studies demonstrate that the monomeric, globular C-terminal domain of Pat1
203 can bind helical leucine motifs (HLMs) in the disordered C-terminus of Dcp2 (Charenton
204 et al. 2017; Lobel et al. 2019). Known dimeric HLM binding proteins, such as Edc3, can
205 interact with Dcp2 and undergo liquid-liquid phase separation with Dcp2 constructs that
206 contain multiple HLMs (Schutz et al. 2017; Fromm et al. 2014). Our biochemical data
207 demonstrate that PatMC can inherently oligomerize in the absence of RNA, so we tested
208 if it could promote liquid-liquid phase separation with multivalent Dcp1/Dcp2 complexes,
209 analogous to Edc3. PatMC was purified fused to maltose-binding protein (MBP) to
210 enhance its solubility (see Methods). It was then mixed with a Dcp2 construct containing
211 both the catalytic core and three HLMs in the disordered C-terminus extension, along with
212 its obligate cofactor Dcp1 (Dcp1/Dcp2 1-504, termed Dcp1/Dcp2$_{Ext}$) **(Fig. 5A)**. Though
213 neither PatMC nor Dcp1/Dcp2$_{Ext}$ formed condensates individually, mixing stoichiometric
214 amounts of Dcp1/Dcp2$_{Ext}$ with MBP-PatMC resulted in formation of phase separated
215 droplets (**Fig. 5B and data not shown)**.

216

217 To understand the requirements of PatMC and Dcp1/Dcp2$_{Ext}$ for droplet formation, we
218 queried how individual regions of both complexes contribute to phase separation. The C-
219 terminal domain of Pat1 is monomeric and binds HLMs, but did not promote phase
220 separation of Dcp1/Dcp2$_{Ext}$ (**Fig. 5B**). Additionally, PatMC did not phase separate with a

Dcp1/Dcp2 complex containing a single HLM (Dcp2 residues 1-266, termed $Dcp2_{HLM1}$) **(Fig. 5B)**. These data suggest that the middle and C-terminal domains of Pat1 promote phase separation of Dcp1/Dcp2 by driving self-association and binding HLMs on Dcp2, respectively. We conclude PatMC oligomerization promotes phase separation with multivalent cofactors such as Dcp2.

PatMC and Dcp2 both interact with RNA, which can trigger or potentiate liquid-liquid phase separation with oligomeric RNA binding proteins (RBPs) (Mugler et al. 2016; Lin et al. 2015). The PatMC/Dcp1/$Dcp2_{Ext}$ droplets were able to incorporate A15 RNA, though A15 RNA did not change the critical concentration required for phase separation (**Fig. 5C & S5A)**. However, neither short A15 RNAs nor poly(A) RNA promoted droplet formation with either PatMC or Dcp1/$Dcp2_{Ext}$ alone (**Fig. 5C and data not shown**). RNA could not trigger phase separation with either Dcp1/$Dcp2_{Ext}$ or PatMC alone, suggesting that the protein-protein interactions are the primary driver of phase separation between PatMC and Dcp2.

We next asked if other mRNA decay factors could be incorporated in PatMC/Dcp1/Dcp2 droplets. Lsm1-7, but not a nonspecific protein, was recruited of pre-formed PatMC/Dcp1/$Dcp2_{Ext}$ condensates, indicating that PatMC can bridge both 5' (Dcp1/Dcp2) and 3' (Lsm1-7) decay factors in the context of the phase separated droplet (**Fig. 5D & S5C**). Lsm1-7 neither phase separates with PatMC nor affected the critical concentration for droplet formation, consistent with Lsm1-7 being a monomeric complex (**Fig. S5A &**

S5B). Furthermore, Dcp1/Dcp2$_{Ext}$/PatMC/Lsm1-7 condensates recruited RNA (**Fig. 5SD**). These observations suggest that Pat1 may bridge both 5' and 3' activities in the context of a phase separated droplet.

DISCUSSION

Our biochemical reconstitution uncovers how Pat1 broadens the specificity of the Lsm1-7 complex and promotes higher order assembly of multiple mRNA decay factors. First, Pat1 expands the Lsm1-7 complex's sequence preference by enhancing binding to adenine-rich RNAs. Second, PatMC promotes cooperative binding of Lsm1-7 to RNA, which drives oligomerization on nucleic acid. Third, the PatMC/Lsm1-7 complex has the inherent ability to oligomerize, which is dependent on Pat1 and consistent with coimmunoprecipitation data in fission yeast (Wang et al. 2017). Finally, we show that an oligomeric PatMC drives phase separation with multivalent Dcp1/Dcp2 complexes that can recruit RNA and additional decay factors to droplets. Taken together, this biochemically reconstituted system reveals how Pat1 increases the range of RNA targets bound by the Lsm1-7 complex and facilitates higher order assembly of multiple decapping factors (**Fig. 6A/B)**.

The Lsm1-7 ring is the high affinity RNA binding component of the Pat1/Lsm1-7 complex and has a preference for U-rich oligonucleotides (Wu et al. 2014; Lobel et al. 2019; Chowdhury et al. 2007). Pat1 broadens the specificity of the Lsm1-7 complex by enhancing the affinity of Lsm1-7 for oligonucleotides with higher adenine content (Lobel

et al. 2019; Chowdhury et al. 2013) (**Fig. 1**). Because PatMC does not bind RNA with appreciable affinity on its own, we suggest that Pat1 may allow the Lsm1-7 complex to bind sequences which it has inherently weaker affinity for and therefore expand the complex's target repertoire (Lobel et al. 2019) (**Fig. S1G**).

Though PatMC increases the range of RNA substrates bound by Lsm1-7, it is unclear if all RNA targets bind in the same manner. For example, PatMC does not enhance the affinity of Lsm1-7 for U15 RNA, in contrast to A15 RNA or A/U rich RNA. Moreover, higher adenine contents favor more cooperative binding of PatMC/Lsm1-7. On the other hand, Pat1/Lsm1-7 stoichiometrically binds all RNA targets as a stable dimer. While we observe tetramers with 15mer RNAs, these assemblies are less stable than the dimeric species (**Fig. 2 & Fig. S2)** Determining the binding modes of different RNAs with the Pat1/Lsm1-7 complex remains a challenge for future structural studies.

PatMC also consistently increased the cooperativity of Lsm1-7 binding to all oligonucleotides tested, suggesting a coupling between protein-protein interactions and RNA binding. In support, addition of RNAs drive formation of stable dimeric PatMC/Lsm1-7 assembly whereas in the absence of RNA, PatMC/Lsm1-7 exists in monomer/dimer equilibrium. This suggests two possible pathways which the PatMC/Lsm1-7 complex can load onto RNA. First, RNA may bind to dimeric PatMC/Lsm1-7 from a pre-existing monomer/dimer equilibrium. Alternatively, RNA could bind monomeric PatMC/Lsm1-7

286 which then forms a dimer (**Fig. 6A**). These pathways, could in fact, be part of a
287 thermodynamic cycle, which is in qualitative agreement with our observations.
288
289 The inherent ability of PatMC to oligomerize drives phase separation with multivalent
290 cofactors, such as Dcp2 containing multiple HLMs. This derives from multivalent
291 interactions between Dcp2 and oligomeric PatMC. These droplets can recruit Lsm1-7,
292 providing evidence that Pat1 can bring both 5' and 3' mRNA decay factors in close
293 proximity in the context of these phase separated droplets (**Fig. 5**). Additional partners of
294 Pat1, such as Dhh1, may cooperate to further promote droplet formation (Sachdev et al.
295 2019). Nucleating high local concentration of multiple decapping RBPs in the context of
296 a phase separated droplet may be leveraged for 5' and 3' end communication during
297 decay (**Fig. 6B**). Future work is required to understand how an oligomeric Pat1 is
298 regulated and functions in assembling an active decapping mRNP during 5'-3' mRNA
299 decay.
300
301 The discovery that Pat1 has the ability to oligomerize is reminiscent of the homo-
302 hexameric bacterial Lsm-family protein, Hfq, and its cofactor Crc. Recent work has
303 demonstrated that two copies of Crc can bridge two Hfq hexamers in an RNA dependent
304 manner (Pei et al. 2019; Sonnleitner et al. 2018). While the details of higher order Lsm
305 assemblies between bacteria and eukaryotes differ, oligomerization may be a conserved
306 feature of Lsm complexes and their cofactors.
307

MATERIALS AND METHODS

Protein expression and purification

All proteins were expressed in BL21(DE3)* (Thermofisher) cells in LB media. Cells were grown to OD_{600} = 0.6 at 37 °C, after which IPTG was added to 1 mM. Cells were then grown overnight at 18 °C for 16 hours. For expression of copurified PatMC/Lsm1-7, a polycistron containing all seven Lsm proteins was cloned into site one of a pET-Duet vector, with an N-terminal hexahistidine tag followed by a TEV cleavage sequence on Lsm1. A codon optimized PatMC (residues 296-754) was ordered from IDT and cloned into site two of the pET-Duet vector. Cells were harvested by centrifugation and lysed in appropriate buffer. For Lsm1-7 and PatMC/Lsm1-7 complexes, cells were lysed in Buffer A (2 M NaCl, 20 mM HEPES pH 7.5, 20 mM Imidazole, 5 mM βME, protease inhibitor (Roche)) by sonication. Lysate was subsequently clarified by centrifugation and the supernatant was bound to Ni-NTA resin (GE) at 4 °C for 1 hour. The resin was then transferred to a gravity column and washed with 20 column volumes of Buffer A before being eluted in 25 mL of Buffer E (250 mM NaCl, 250 mM Imidazole, 20 mM HEPES pH 7.0, 10 mM βME). The elution was then loaded directly onto a 5 mL HiTrap Heparin column (GE). The heparin column was run at 2 ml/min from a 0.25-1 M NaCl gradient over 20 column volumes. Fractions containing the appropriate protein complex were concentrated in 30 kD concentrators (Amicon) to ~2 mL before adding TEV overnight at 4 °C. The following day, the sample was filtered and further purified by gel filtration using a Superdex 200 16/60 column (GE). Coexpressed PatMC/Lsm1-7 was purified in 400 mM

NaCl, 20 mM HEPES 7.0, 1 mM DTT and Lsm1-7 alone was purified in 150 mM NaCl, 20 mM HEPES pH 7.0, 1 mM DTT. Fractions containing protein were concentrated before being flash frozen and stored at -80 °C.

All MBP-Pat1 fusions were purified as described previously (Lobel et al. 2019). For Spycatcher purification, a C-terminal KCK tag was added (SpycatcherKCK) and purified similar to the MBP-Pat1 fusions, with the heparin step omitted. SpycatcherKCK was purified on Superdex 75 16/60 column in 150 mM NaCl, 20 mM HEPES pH 7.0, 0.5 mM TCEP.

Fluorescence polarization

All fluorescent polarization experiments were performed in 200 mM NaCl, 20 mM HEPES pH 7.0, 1 mM DTT, 5 mM $MgCl_2$ with 0.3 μg/ul Acetylated BSA (Promega) . All RNAs used were labelled with 5' FAM (IDT) and were used at final concentration of 500 pM. All binding curves were fit to the following Hill model for single site binding:

$$Y(mp) = (\max(mp) - \min(mp)) * \frac{[protein]^n}{[protein]^n + {K_d}^n} + \min(mp)$$

To determine the ΔG of binding, each independent replicate was fitted to the above model and ΔG was determined by the relationship $\Delta G = +RT*\ln(K_d)$. The ΔG from each individual fit was averaged and plotted with standard deviation. Hill coefficients were averaged from fitting three separate binding isotherms and shown with standard deviation.

For analysis of stoichiometry, 5'-FAM RNA was kept at 0.5 μM in the same buffer as used for the fluorescence polarization assay. Protein was titrated into solution containing labelled RNA and fluorescence polarization was measured for each concentration. The linear portion was fit to a linear model and the average of the last four points were used to fit a line at the saturation point. The intersection of these two lines was used to determine the binding stoichiometry.

Analytical Size Exclusion Chromatography (SEC) and SEC-MALS

Analytical SEC was performed in buffer M (250 mM NaCl, 20 mM HEPES pH 7.0, 1 mM DTT), or in the appropriate NaCl concentration. Samples were mixed at ~30 μM and incubated for 15 minutes in 350 mM NaCl, 20 mM HEPES pH 7.0, 1 mM DTT on ice before being filtered and injected onto a GE Superdex 200 10/300-Increase analytical size exclusion column. When appropriate, samples were mixed with 1.1-fold molar excess RNA. All samples were run at 0.35 ml/min, and peaks were analyzed by SDS-PAGE (Invitrogen). For experiments involving reinjection of fractions over SEC, 500 μl of fractions were spin filtered before reinjecting over SEC.

For SEC-MALS, 165 μg of sample was filtered through a 0.1 μm spin filter (Amicon) before being injected onto a pre-equilibrated KW-804 column (Shodex, New York, New York). For samples with RNA, stoichiometric amounts of RNA were added prior to spin filtration. Data was acquired with an inline DAWN HELEOS MALS and Optilab rEX differential

refractive index detector (Wyatt Technology, Santa Barbara, CA). All analysis was performed using ASTRA VI software (Wyatt Technology). Data was then exported and plotted with R.

Analytical ultracentrifugation

Sample was buffer exchanged into buffer M using Zeba spin columns (Thermofisher) and diluted to 9.3 μM. When appropriate, stoichiometric amounts of RNA were added to the sample after buffer exchange. AUC cells were assembled according to manufacturer's protocol and 100 μl of sample was loaded into the cell. The sample was incubated at 22 °C for >2 hours prior to centrifugation. Samples were run at 30,000 rpm for 10-12 hours in a Beckman XL/A analytical ultracentrifuge. Scans for samples containing only protein were collected at 280 nm, and samples containing RNA were scanned at both 280 and 260 nm. Sedimentation velocity analysis was performed in SEDFIT (NIH) and plots were generated with GUSSI (Schuck 2003; Brautigam 2015). Experimental parameters were determined using SEDNTERP (NIH). The following parameters were used for fitting: partial volume, 0.739818; buffer density, 1.0101; buffer viscosity, 0.0104032.

Protein labelling

For labelling with dyes, proteins were buffer exchanged into appropriate labelling buffer using Zeba spin columns (Thermofisher). Lsm1-7 and SpycatcherKCK were labelled with 5-fold molar excess Alexa Fluor 555 maleimide for one hour at room temperature in 150 mM NaCl, 20 mM HEPES pH 7.5, 0.5 mM TCEP. Reactions were quenched by addition

of βME to a final concentration of 10 mM. MBP-PatMC was labelled with 4-fold molar excess NHS-Fluorescein (Thermofisher) for 1 hour at room temperature in 150 mM NaCl, 150 mM Sodium bicarbonate pH 8.4 before being quenched by adding TRIS-HCl pH 8.0 to a final concentration of 50 mM. All quenching steps were performed at room temperature for 20 minutes. Free dye was separated from labelled protein by Illustra NICK columns (GE) according to the manufacturer's instruction. Labelling efficiency and concentrations were calculated by UV-vis spectroscopy.

Microscopy

All images were acquired with Nikon Eclipse T*i* equipped with a 40x dry lens. Samples were prepared in a 384 well plate (Greiner) that was cleaned with 0.1M NaOH and passivated with PEG-silane and 100 mg/ml BSA (Sigma-Aldrich) before being washing with water to remove residual BSA. Proteins or RNA were mixed at specified concentrations in a final buffer concentration of 60 mM NaCl, 20 mM HEPES pH 7.0, 1 mM DTT. When appropriate, dye-labelled protein or RNA were added to 100 nM. Samples were incubated at room temperature for 20 minutes prior to imaging. Images were analyzed in FIJI (Schindelin et al. 2019).

ACKNOWLEDGEMENTS

We thank Alexandra Rizo and Serena Sanulli for experimental guidance, the Nikon Imaging Center at UCSF for use of the microscope, Daniel Southworth's lab for use of

417 SEC-MALS, and Ryan Tibble and Nathan Gamarra for comments on the manuscript. This
418 work was supported by US National Institutes of Health grant R01GM078360 to J.D.G.

419

420 **REFERENCES**

421 Banani SF, Lee HO, Hyman AA, Rosen MK. 2017. Biomolecular condensates:
422 Organizers of cellular biochemistry. *Nat Rev Mol Cell Biol* **18**: 285–298.
423 Bonnerot C, Boeck R, Lapeyre B. 2000. The Two Proteins Pat1p (Mrt1p) and Spb8p
424 Interact In Vivo, Are Required for mRNA Decay, and Are Functionally Linked to
425 Pab1p. *Mol Cell Biol* **20**: 5939–5946.
426 Bouveret E, Rigaut G, Shevchenko A, Wilm M, Séraphin B. 2000. A Sm-like protein
427 complex that participates in mRNA degradation. *EMBO J* **19**: 1661–1671.
428 Brautigam CA. 2015. Calculations and Publication- Quality Illustrations for Analytical
429 Ultracentrifugation Data. *Methods Enzymol* **562**: 109–133.
430 Chang H, Lim J, Ha M, Kim VN. 2014. TAIL-seq: Genome-wide Determination of
431 Poly(A) Tail Length and 3' End Modifications. *Mol Cell* **53**: 1044–1052.
432 Charenton C, Gaudon-Plesse C, Fourati Z, Taverniti V, Back R, Kolesnikova O,
433 Séraphin B, Graille M. 2017. A unique surface on Pat1 C-terminal domain directly
434 interacts with Dcp2 decapping enzyme and Xrn1 5′–3′ mRNA exonuclease in
435 yeast. *Proc Natl Acad Sci* **114**: E9493–E9501.
436 Chowdhury A, Kalurupalle S, Tharun S. 2013. Pat1 contributes to the RNA binding
437 activity of the Lsm1-7 – Pat1 complex. *RNA* **20**: 1465–1475.
438 Chowdhury A, Mukhopadhyay J, Tharun S. 2007. The decapping activator Lsm1p-7p-

Pat1p complex has the intrinsic ability to distinguish between oligoadenylated and polyadenylated RNAs. *RNA* **13**: 998–1016.

Fromm SA, Kamenz J, Noldeke ER, Neu A, Zocher G, Sprangers R. 2014. In vitro reconstitution of a cellular phase-transition process that involves the mRNA decapping machinery. *Angew Chemie - Int Ed* **53**: 7354–7359.

He F, Celik A, Wu C, Jacobson A. 2018. General decapping activators target different subsets of inefficiently translated mRNAs. *Elife* **7**: 1–30.

Hubstenberger A, Courel M, Bénard M, Souquere S, Ernoult-Lange M, Chouaib R, Yi Z, Morlot JB, Munier A, Fradet M, et al. 2017. P-Body Purification Reveals the Condensation of Repressed mRNA Regulons. *Mol Cell* **68**: 144–157.e5.

Jonas S, Izaurralde E. 2015. Towards a molecular understanding of microRNA-mediated gene silencing. *Nat Rev Genet* **16**: 421–433.

Kurosaki T, Popp MW, Maquat LE. 2019. Quality and quantity control of gene expression by nonsense- mediated mRNA decay. *Nat Rev Mol Cell Biol* **20**: 406–420.

Lim J, Ha M, Chang H, Kwon SC, Simanshu DK, Patel DJ, Kim VN. 2014. Uridylation by TUT4 and TUT7 marks mRNA for degradation. *Cell* **159**: 1365–1376.

Lin Y, Protter DSW, Rosen MK, Parker R. 2015. Formation and Maturation of Phase-Separated Liquid Droplets by RNA-Binding Proteins. *Mol Cell* **60**: 208–219.

Lobel JH, Tibble RW, Gross JD. 2019. Pat1 activates late steps in mRNA decay by multiple mechanisms. *Proc Natl Acad Sci* **116**: 23512–23517.

Mitchell SF, Jain S, She M, Parker R. 2012. Global analysis of yeast mRNPs. *Nat Struct*

Mol Biol **20**: 127–133.

Moore MJ. 2005. From birth to death: The complex lives of eukaryotic mRNAs. *Science (80-)* **309**: 1514–1518.

Mugler CF, Hondele M, Heinrich S, Sachdev R, Vallotton P, Koek AY, Chan LY, Weis K. 2016. ATPase activity of the DEAD-box protein Dhh1 controls processing body formation. *Elife* **5**.

Mugridge JS, Coller J, Gross JD. 2018. Structural and molecular mechanisms for the control of eukaryotic 5′–3′ mRNA decay. *Nat Struct Mol Biol* **25**.

Mullen TE, Marzluff WF. 2008. Degradation of histone mRNA requires oligouridylation followed by decapping and simultaneous degradation of the mRNA both 5' to 3' and 3' to 5'. *Genes Dev* **22**: 50–65.

Nissan T, Rajyaguru P, She M, Song H, Parker R. 2010. Decapping Activators in Saccharomyces cerevisiae Act by Multiple Mechanisms. *Mol Cell* **39**: 773–783.

Pei XY, Dendooven T, Sonnleitner E, Chen S, Luisi BF. 2019. Architectural principles for Hfq / Crc- mediated regulation of gene expression. *Elife* **8**: 1–20.

Pilkington GR, Parker R. 2008. Pat1 Contains Distinct Functional Domains That Promote P-Body Assembly and Activation of Decapping. *Mol Cell Biol* **28**: 1298–1312.

Rissland OS, Norbury CJ. 2009. Decapping is preceded by 3' uridylation in a novel pathway of bulk mRNA turnover. *Nat Struct Mol Biol* **16**.

Sachdev R, Hondele M, Linsenmeier M, Vallotton P, Mugler CF, Arosio P, Weis K, Zurich ETH. 2019. Pat1 promotes processing body assembly by enhancing the

phase separation of the DEAD-box ATPase Dhh1 and RNA. *Elife* **8**: 1–27.

Schindelin J, Arganda-carreras I, Frise E, Kaynig V, Longair M, Pietzsch T, Preibisch S, Rueden C, Saalfeld S, Schmid B, et al. 2019. Fiji : an open-source platform for biological-image analysis. *Nat Methods* **9**.

Schuck P. 2003. On the analysis of protein self-association by sedimentation velocity analytical ultracentrifugation. *Anal Biochem* **320**: 104–124.

Schutz S, Noldeke ER, Sprangers R. 2017. A synergistic network of interactions promotes the formation of in vitro processing bodies and protects mRNA against decapping. *Nucleic Acids Res* **45**: 6911–6922.

Sharif H, Ozgur S, Sharma K, Basquin C, Urlaub H, Conti E. 2013. Structural analysis of the yeast Dhh1-Pat1 complex reveals how Dhh1 engages Pat1, Edc3 and RNA in mutually exclusive interactions. *Nucleic Acids Res* **41**: 8377–8390.

Sheth U, Parker R. 2003. Decapping and decay of messenger RNA occur in cytoplasmic processing bodies. *Science (80-)* **300**: 805–808.

Sonnleitner E, Wulf A, Pei X, Wolfinger T, Forlani G, Prindl K, Abdou L, Resch A, Allain H, Luisi BF, et al. 2018. Interplay between the catabolite repression control protein Crc , Hfq and RNA in Hfq-dependent translational regulation in Pseudomonas aeruginosa. *Nucleic Acids Res* **46**: 1470–1485.

Stevens A. 1980. Purification and characterization of a Saccharomyces cerevisiae exoribonuclease which yields 5'-mononucleotides by a 5' -3' mode of hydrolysis. *J Biol Chem* **255**: 3080–5.

Teixeira D, Parker R. 2007. Analysis of P-Body Assembly in Saccharomyces

505 Cerevisiae. *Mol Biol Cell* **18**: 2274–2287.

506 Tharun S, He W, Mayes AE, Lennertz P, Beggs JD, Parker R. 2000. Yeast Sm-like
507 proteins function in mRNA decapping and decay. *Nature* **404**: 515–518.

508 Tharun S, Parker R. 2001. Targeting an mRNA for decapping: Displacement of
509 translation factors and association of the Lsm1p-7p complex on deadenylated yeast
510 mRNAs. *Mol Cell* **8**: 1075–1083.

511 Vindry C, Marnef A, Broomhead H, Twyffels L, Ozgur S, Stoecklin G, Llorian M, Smith
512 CW, Mata J, Weil D, et al. 2017. Dual RNA Processing Roles of Pat1b via
513 Cytoplasmic Lsm1-7 and Nuclear Lsm2-8 Complexes. *Cell Rep* **20**: 1187–1200.

514 Wang C-Y, Wang Y-T, Hsiao W-Y, Wang S-W. 2017. Involvement of fission yeast Pdc2
515 in RNA degradation and P-body function. *RNA* **23**: 493–503.

516 Webster MW, Chen Y, Stowell JAW, Alhusaini N, Sweet T, Graveley BR, Coller J,
517 Passmore LA. 2018. mRNA Deadenylation Is Coupled to Translation Rates by the
518 Differential Activities of Ccr4-Not Nucleases. *Mol Cell* **70**: 1089–1100.

519 Wu D, Muhlrad D, Bowler MW, Jiang S, Liu Z, Parker R, Song H. 2014. Lsm2 and Lsm3
520 bridge the interaction of the Lsm1-7 complex with Pat1 for decapping activation.
521 *Cell Res* **24**: 233–246.

522 Wyatt PJ. 1993. Light scattering and the absolute characterization of macromolecules.
523 *Anal Chim Acta* **272**.

524 Xing W, Muhlrad D, Parker R, Rosen MK. 2018. A quantitative inventory of yeast P
525 body proteins reveals principles of compositional specificity. *bioRxiv*.

526 Yi H, Park J, Ha M, Lim J, Chang H, Kim VN. 2018. PABP Cooperates with the CCR4-

527 NOT Complex to Promote mRNA Deadenylation and Block Precocious Decay. *Mol*
528 *Cell* **70**: 1081–1088.

529

530 **FIGURE LEGENDS**

531 **Figure 1: PatMC enhances Lsm1-7 binding to Adenine-rich substrates in a**
532 **cooperative manner.**

533 **A,** Schematic of Pat1 domains and Lsm1-7 **B,** SDS-PAGE of the Lsm1-7 complex alone
534 (left) or with PatMC (right). Molecular weight (kDa) shown on right. **C,** Lsm1-7 or
535 PatMC/Lsm1-7 binding to different 5'-FAM labelled 15mer RNAs (A15, A14U1, A10U5,
536 U5A10, U10A5, U15) monitored by fluorescence polarization. Numbers correspond to
537 labels in **D**. Binding affinities were converted to ΔG and plotted against the fractional uracil
538 content of the oligonucleotides (n=3). **D,** Hill coefficients for each fit for the binding
539 isotherms shown in **C** (n=3).

540

541 **Figure 2: RNA promotes stable dimerization of the PatMC/Lsm1-7 complex.**

542 **A-B,** SEC-MALS of 20.6 μM PatMC/Lsm1-7 with **A,** A15 and **B,** A10. Expected and
543 observed molar masses are shown in Table 1. **C,** SV-AUC of 9.3 μM PatMC/Lsm1-7 with
544 stoichiometric amounts of A15 RNA at 250 mM NaCl. c(S) is the sedimentation
545 distribution with molecular weights determined from fits.

546

547 **Figure 3: Multiple RNA sequences drive higher order PatMC/Lsm1-7 assembly in a**
548 **Pat1 dependent manner.**

549 **A,** SEC-MALS of 20.6 μM PatMC/Lsm1-7 with U15 RNA. The expected molar mass of
550 the monomeric PatMC/Lsm1-7 complex is 133 kDa. **B,** Representative SDS-PAGE gel of
551 fractions in **A. C,** SEC-MALS of 20.6 μM Lsm1-7 with U15 RNA. The expected mass of
552 the monomeric Lsm1-7 complex is 81 kDa. Expected and observed molar masses are
553 shown in Table 1. **D,** Stoichiometry analysis of Lsm1-7 or PatMC/Lsm1-7 with 5'-FAM
554 labelled U15 RNA at 0.5 μM, which is >100-fold above K_d.
555
556 **Figure 4: The PatMC/Lsm1-7 complex can intrinsically form a dimeric complex.**
557 **A,** Preparative size exclusion chromatography of the PatMC/Lsm1-7 complex in a 400
558 mM NaCl buffer. **B,** SEC-MALS of the concentrated PatMC/Lsm1-7 complex at 250 mM
559 NaCl. The expected mass of the monomeric PatMC/Lsm1-7 complex is 133 kDa.
560 Expected and observed molar masses are shown in Table 1. **C,** Representative SDS-
561 PAGE gel of peaks (Left to right: earlier to later elution volumes). **D,** SV-AUC of 9.3 μM
562 PatMC/Lsm1-7 at 250 mM NaCl. c(S) is the sedimentation distribution with molecular
563 weights determined from fits.
564
565 **Figure 5: Oligomerization of PatMC promotes liquid-liquid phase separation with**
566 **Dcp2 and recruitment of additional RNA decay machinery.**
567 **A,** Schematic of Dcp2 construct used. Purple represents the globular domain that cleaves
568 the m7G cap. Gray bars represent helical leucine motifs in the disordered C-terminal
569 extension. **B,** Brightfield and fluorescence microscopy of droplets with 2.5 μM Pat
570 constructs (0.1 μM FITC-labeled) with stoichiometric amounts of Dcp1/$Dcp2_{Ext}$. **C,**

571 Brightfield and fluorescence microscopy of droplets with 2.5 μM PatMC and 2.5 μM rA15
572 RNA or 13.4 ng/μl poly(A) RNA with or without 2.5 μM Dcp1/Dcp2$_{Ext}$ and 0.1 μM FAM-
573 rA15. **D,** Brightfield and fluorescence microscopy of 2.5 μM PatMC (0.1 μM FITC-labelled)
574 and Dcp1/Dcp2$_{Ext}$ with 0.1 μM Alexa555 labelled Lsm1-7. All images taken at 40x
575 magnification. Scale bar, 10 μm.
576
577 **Figure 6: Model for how Pat1 increases specificity and assembly for different**
578 **mRNA decay factors**
579 **A,** Proposed thermodynamic coupling between Pat1 (blue), Lsm1-7 (red), and RNA
580 binding to promote multimerization of the Pat1/Lsm1-7 complex. **B,** Binding of oligomeric
581 Pat1 assemblies to multivalent Dcp1/Dcp2 complexes promotes phase separation and
582 recruitment of additional mRNA decay factors.
583
584 **TABLE LEGENDS**
585 **Table 1: Expected and observed molar masses from SEC-MALS.**
586 Expected and observed molar masses of SEC-MALS chromatograms. Error is displayed
587 in parenthesis to the right of observed peak. Peak 1 and 2 refers to the earlier and later
588 elution volume peaks, respectively.
589
590
591
592

SUPPLEMENTAL FIGURE LEGENDS

Supplemental Figure 1: Binding of Lsm1-7 +/- PatMC to different RNAs

A-F, Lsm1-7 or PatMC/Lsm1-7 binding to **A,** A15 **B,** A14U1 **C,** A10U5 **D,** U5A10 **E,** A5U10 **F,** U15 (n = 3 for all). **G,** MBP-PatMC binding to U15 in 150 mM NaCl (n = 2).

Supplemental Figure 2: The dimeric PatMC/Lsm1-7/RNA assembly is stable.

A, Analytical size exclusion chromatography of PatMC/Lsm1-7 with A15 RNA. Peaks corresponding to dimer and tetramer are labelled. **B,** Reinjection of peak corresponding to the dimeric PatMC/Lsm1-7 complex. **C,** Reinjection of the peak corresponding to the tetrameric PatMC/Lsm1-7 complex. All conditions were in a 250 mM NaCl buffer. The 260 and 280 nm absorbances are displayed in red and blue, respectively.

Supplemental Figure 3: PatMC/Lsm1-7 binds A15 stoichiometrically.

Stoichiometry analysis of Lsm1-7 or PatMC/Lsm1-7 with 5'-FAM labelled A15 RNA at 0.5 μM, which is ~100-fold above K_d.

Supplemental Figure 4: The monomer/dimer equilibrium of the PatMC/Lsm1-7 complex is sensitive to ionic strength of solution.

Analytical size exclusion chromatography of PatMC/Lsm1-7 complexes in different ionic strength solutions as indicated in the figure. All protein was run in 20 mM HEPES pH 7.0, 1 mM DTT and the specified NaCl concentration.

615 **Supplemental Figure 5: The multivalent PatMC/Dcp2$_{Ext}$ interaction is required for**
616 **liquid-liquid phase separation.**

617 **A,** Brightfield images of serial dilutions of droplets containing MBP-PatMC/Dcp1/Dcp2$_{Ext}$
618 with A15 RNA or Lsm1-7. (0.1 μM MBP-PatMC labelled). **B,** Brightfield images of 2.5 μM
619 PatMC and Lsm1-7 **C,** Brightfield and fluorescence microscopy of 2.5 μM MBP-PatMC
620 and Dcp1/Dcp2$_{Ext}$ with 0.1 μM Alexa555-Spycatcher labelled. **D,** Brightfield and
621 fluorescence microscopy of 2.5 μM MBP-PatMC/Dcp1/Dcp2$_{Ext}$/Lsm1-7 droplets with 0.1
622 μM FAM-rA15 and 0.1 μM Alexa555-Lsm1-7. All images taken at 40x magnification. Scale
623 bar, 10 μm.
624

Figure 1

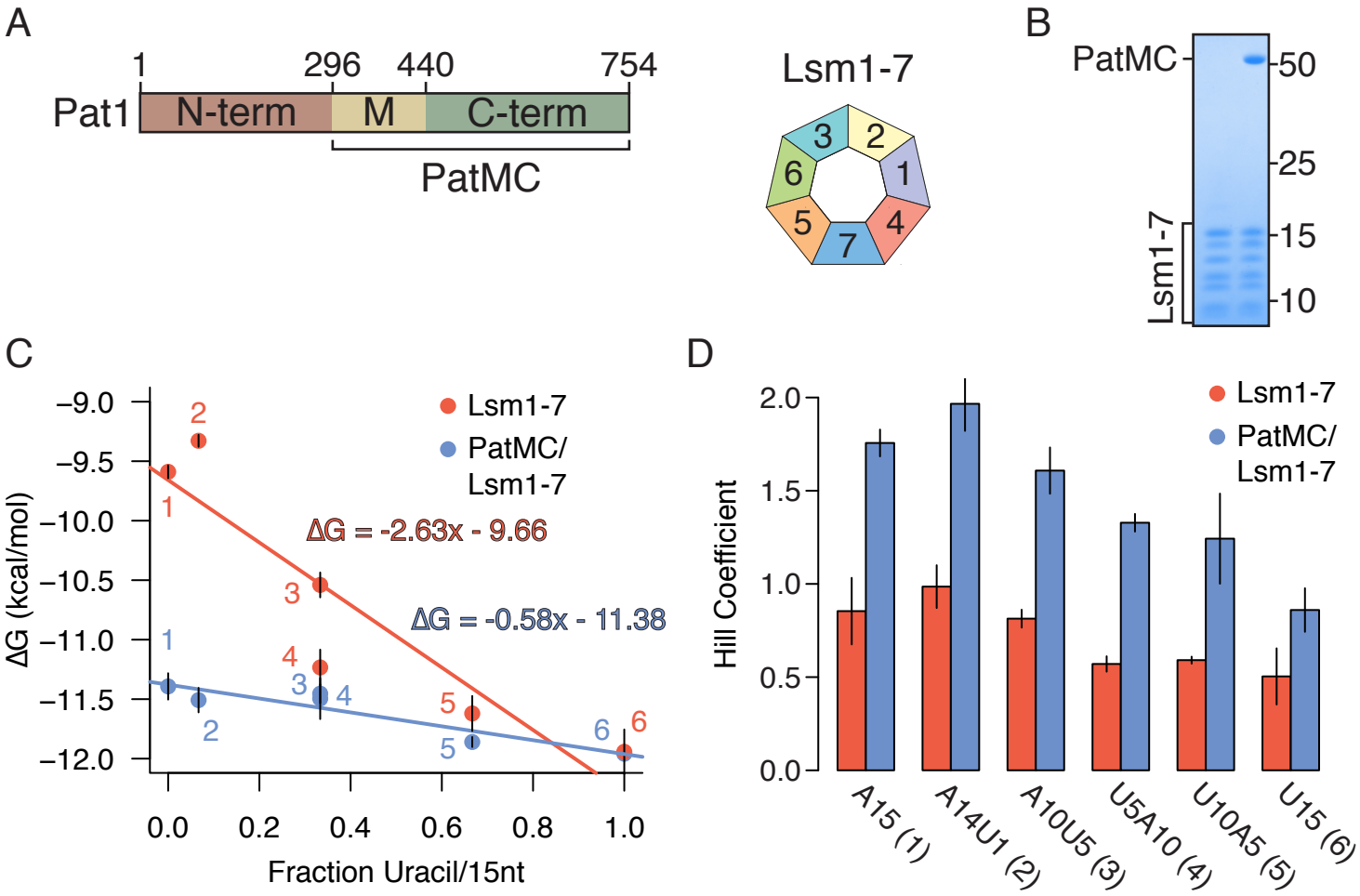

Figure 2

A

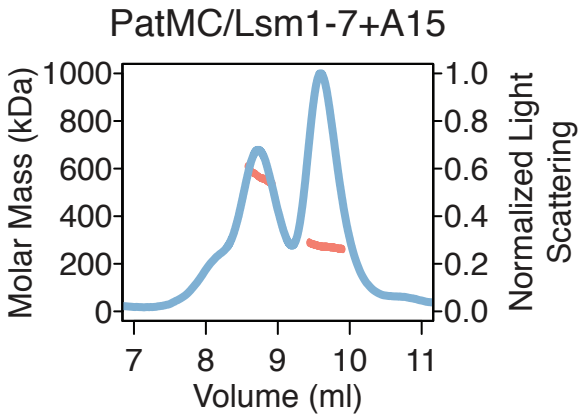

B

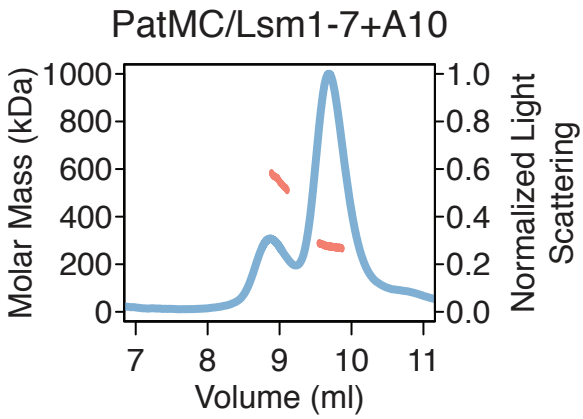

C

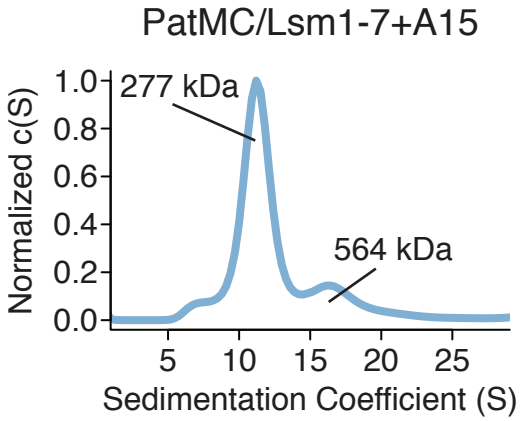

Figure 3

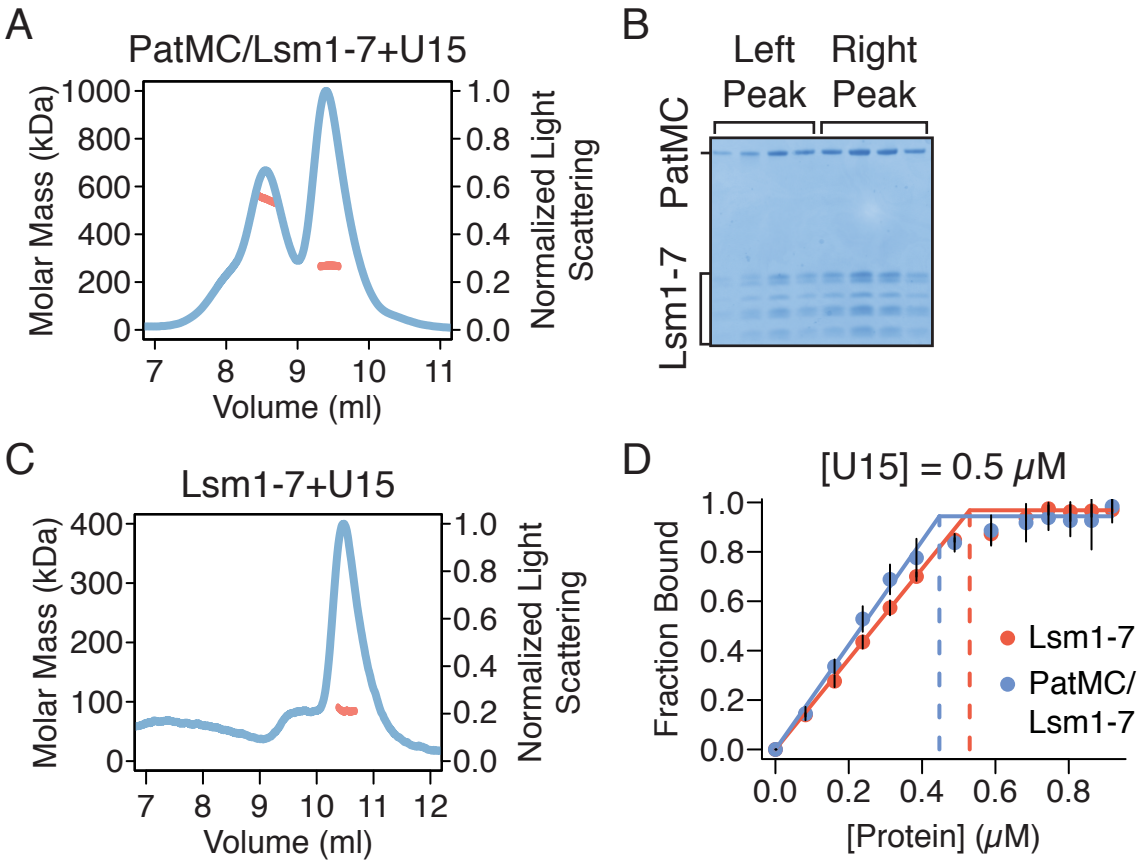

Figure 4

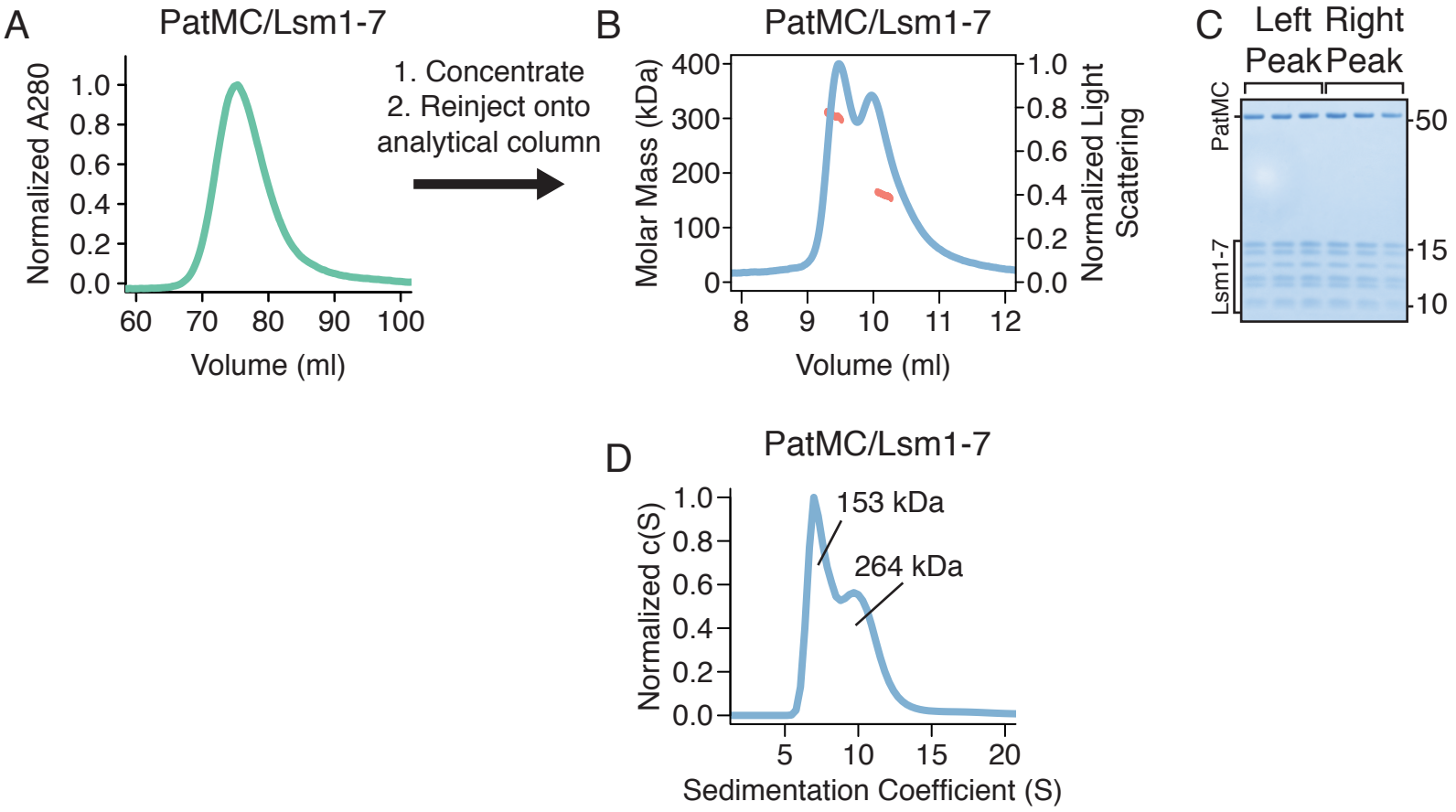

Figure 5

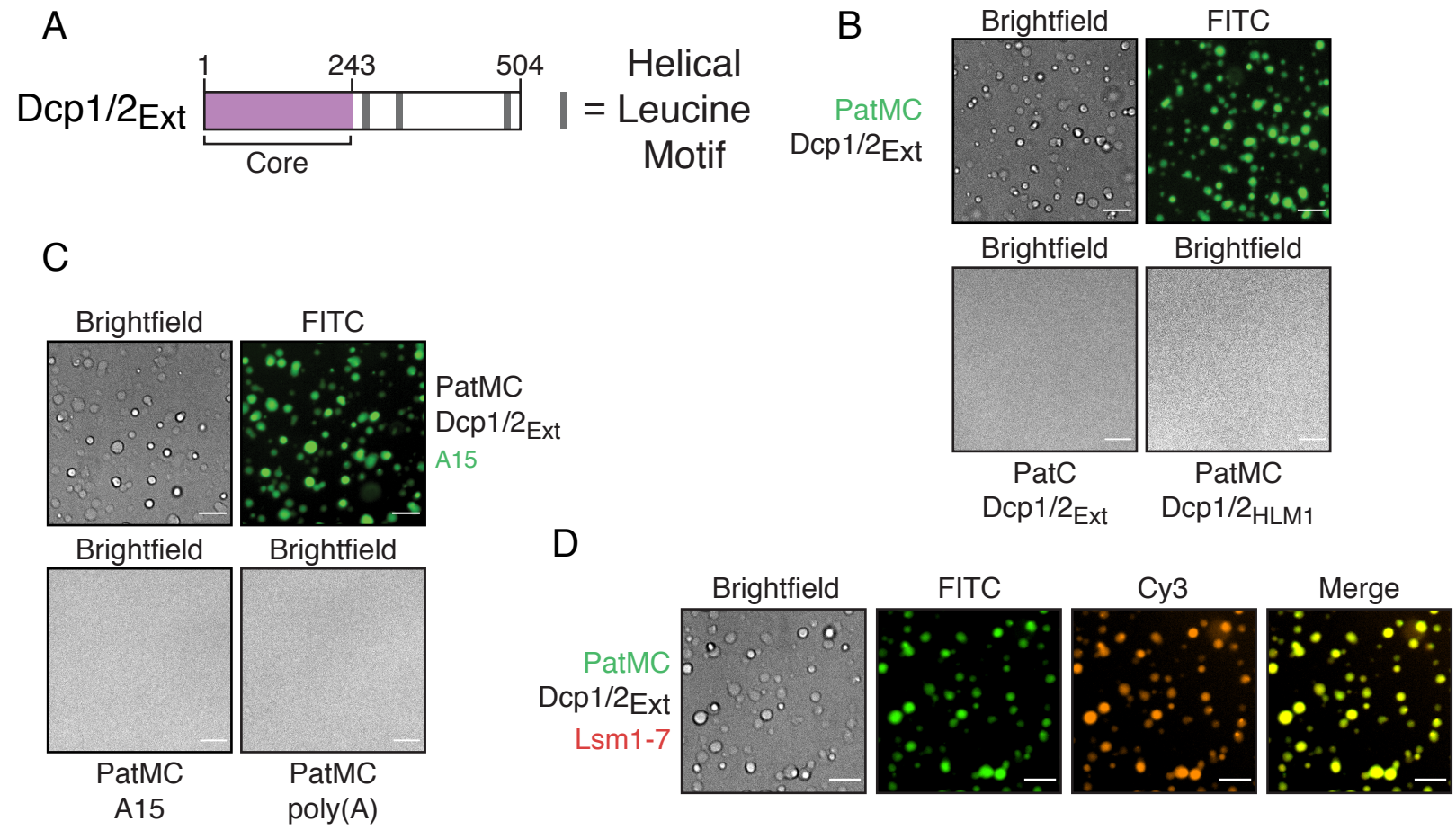

Figure 6

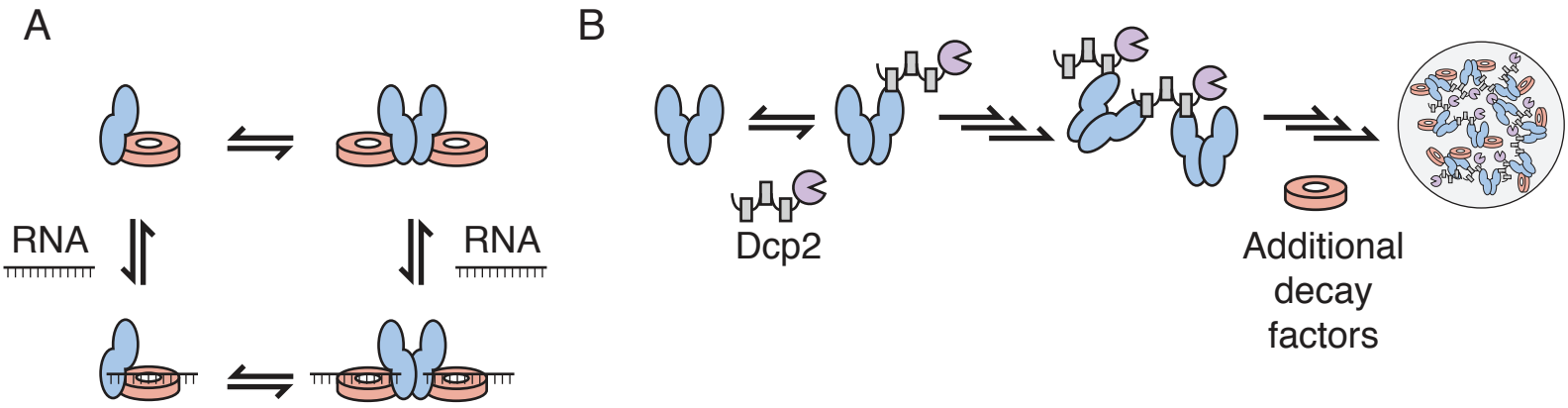

Table 1: Molecular weight determination by SEC-MALS

Protein + RNA Complex	Expected Monomer Molar Mass (kDa)	Observed Molar Mass, Peak 1 (kDa)	Observed Molar Mass, Peak 2 (kDa)
PatMC/Lsm1-7	133.5	304.5 (± 1.20%)	160.3 (± 0.93%)
PatMC/Lsm1-7 + A15	138.2	576.0 (± 1.28%)	273.3 (± 0.56%)
PatMC/Lsm1-7 + A10	136.6	554.2 (± 0.80%)	275.5 (± 0.26%)
PatMC/Lsm1-7 + U15	137.8	548.1 (± 0.91%)	268.1 (± 0.88%)
Lsm1-7 + U15	85.6	86.1 (± 2.40%)	NA

Supplemental Figure 1

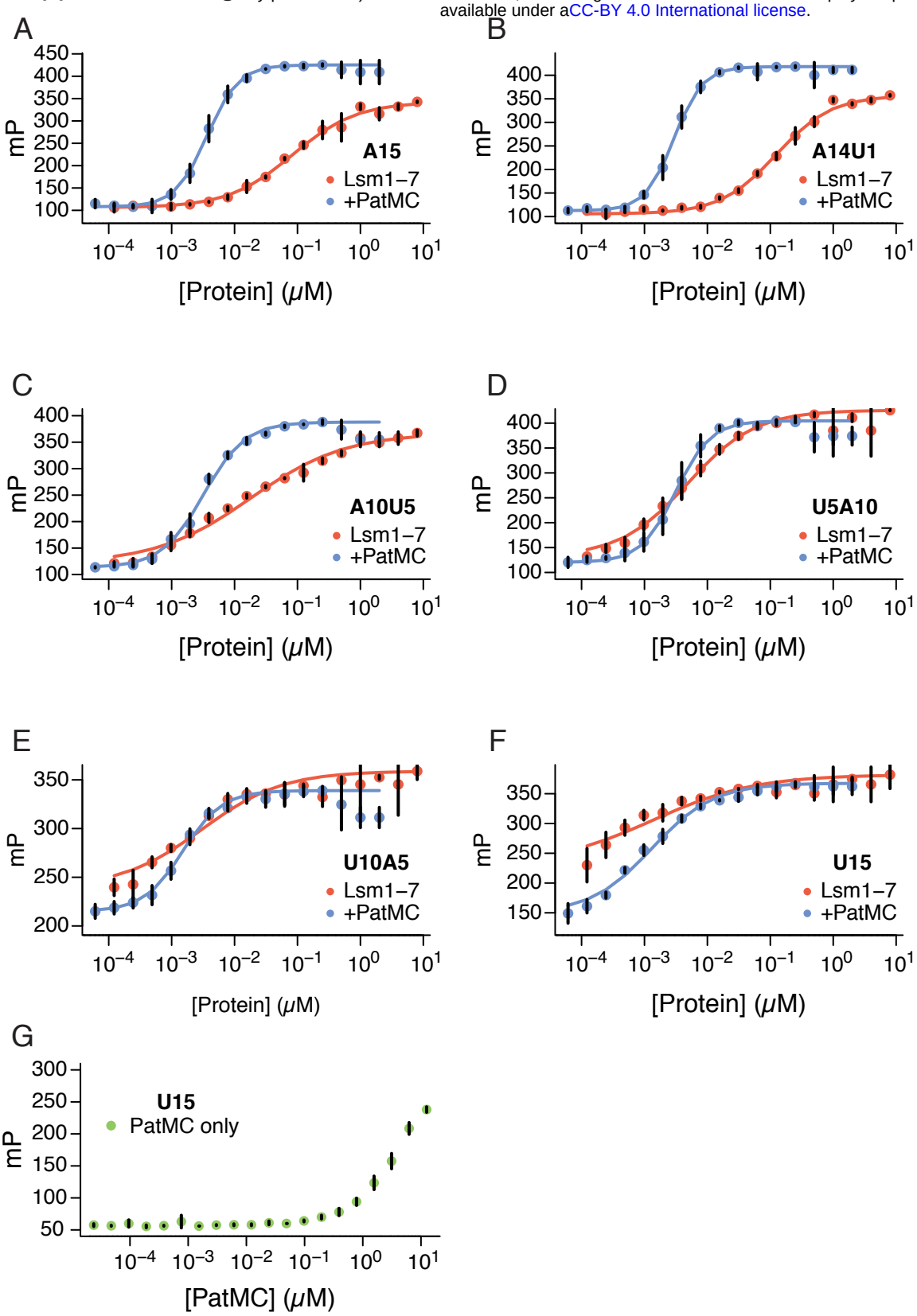

Supplemental Figure 2

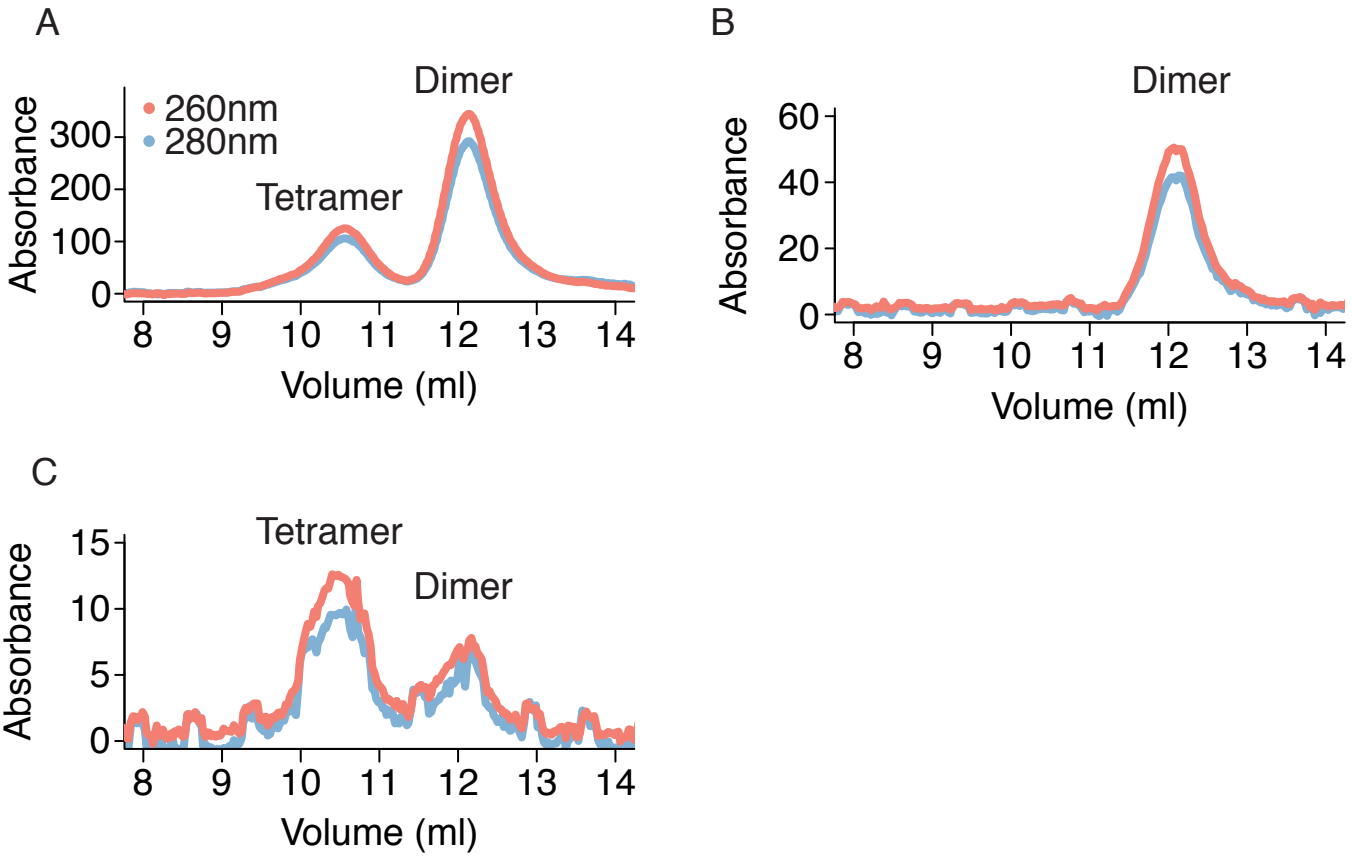

Supplemental Figure 3

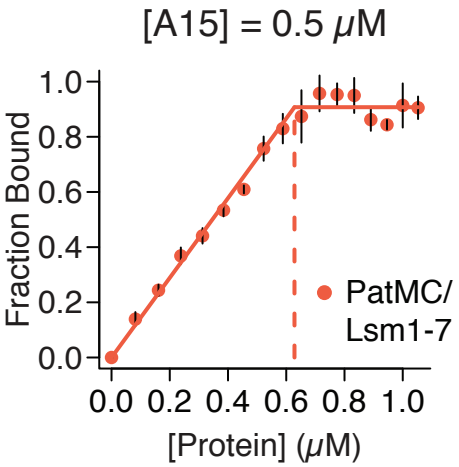

Supplemental Figure 4

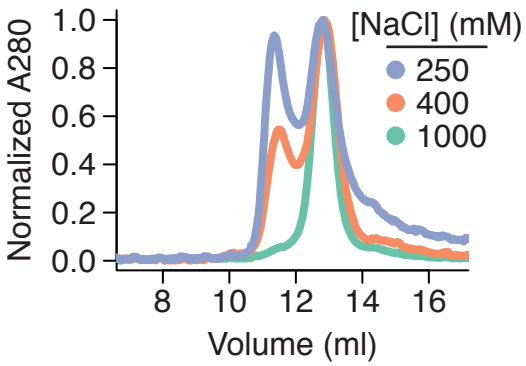

Supplemental Figure 5